

## The Cys3–Cys4 Loop of the Hydrophobin EAS Is Not Required for Rodlet Formation and Surface Activity

Ann H. Kwan<sup>1</sup>, Ingrid Macindoe<sup>1</sup>, Paul V. Vukašin<sup>1</sup>, Vanessa K. Morris<sup>1</sup>, Itamar Kass<sup>2</sup>, Rima Gupte<sup>2</sup>, Alan E. Mark<sup>2</sup>, Matthew D. Templeton<sup>3</sup>, Joel P. Mackay<sup>1</sup> and Margaret Sunde<sup>1\*</sup>

<sup>1</sup>School of Molecular and Microbial Biosciences, University of Sydney, Sydney, New South Wales 2006, Australia

<sup>2</sup>School of Molecular and Microbial Sciences, University of Queensland, St. Lucia, Queensland 4072, Australia

<sup>3</sup>The Horticulture and Food Research Institute of New Zealand, Mt. Albert Research Centre, Auckland 1025, New Zealand

Received 12 May 2008;  
received in revised form  
8 July 2008;  
accepted 11 July 2008  
Available online  
22 July 2008

Class I hydrophobins are fungal proteins that self-assemble into robust amphipathic rodlet monolayers on the surface of aerial structures such as spores and fruiting bodies. These layers share many structural characteristics with amyloid fibrils and belong to the growing family of functional amyloid-like materials produced by microorganisms. Although the three-dimensional structure of the soluble monomeric form of a class I hydrophobin has been determined, little is known about the molecular structure of the rodlets or their assembly mechanism. Several models have been proposed, some of which suggest that the Cys3–Cys4 loop has a critical role in the initiation of assembly or in the polymeric structure. In order to provide insight into the relationship between hydrophobin sequence and rodlet assembly, we investigated the role of the Cys3–Cys4 loop in EAS, a class I hydrophobin from *Neurospora crassa*. Remarkably, deletion of up to 15 residues from this 25-residue loop does not impair rodlet formation or reduce the surface activity of the protein, and the physicochemical properties of rodlets formed by this mutant are indistinguishable from those of its full-length counterpart. In addition, the core structure of the truncation mutant is essentially unchanged. Molecular dynamics simulations carried out on the full-length protein and this truncation mutant binding to an air–water interface show that, although it is hydrophobic, the loop does not play a role in positioning the protein at the surface. These results demonstrate that the Cys3–Cys4 loop does not have an integral role in the formation or structure of the rodlets and that the major determinant of the unique properties of these proteins is the amphipathic core structure, which is likely to be preserved in all hydrophobins despite the high degree of sequence variation across the family.

© 2008 Elsevier Ltd. All rights reserved.

Edited by K. Kuwajima

Keywords: hydrophobin; EAS; rodlets; assembly; amyloid

### Introduction

Hydrophobins are a class of low-molecular-weight proteins (7000–9000 Da) unique to filamentous fungi. They are secreted from fungi as soluble monomers and, upon reaching an interface (e.g., between growth medium and air or between cell wall and air), aggregate

spontaneously to form an amphipathic monolayer. This hydrophobin layer acts as a natural surfactant and reduces the surface tension of the medium, allowing the fungus to breach the water–air interface and to produce hyphae.<sup>1,2</sup> Spores that develop on the end of the aerial structures are coated by a hydrophobin layer that renders their surface hydrophobic and resistant to wetting, thus facilitating their effective dispersal in air.<sup>3</sup> Hydrophobins also play a role in mediating the attachment of fungi to surfaces, such as plant hosts and insect cuticles.<sup>4,5</sup>

All hydrophobins have a large proportion of hydrophobic residues and contain eight cysteines that form four disulfide bonds, including two pairs of adjacent cysteines. The distribution of the cys-

\*Corresponding author. E-mail address: m.sunde@mmb.usyd.edu.au.

Abbreviations used: 1D, one-dimensional; TFA, trifluoroacetic acid; rpHPLC, reversed-phase HPLC; NOE, nuclear Overhauser enhancement; ThT, thioflavin T; NOESY, NOE spectroscopy; MQW, Milli-Q™ water.

teines and the clustering of hydrophobic and hydrophilic residues allow hydrophobins to be grouped into two classes, I and II,<sup>6</sup> and the aggregates formed by these two classes can be distinguished on the basis of their solubility and morphology. Class I aggregates are extremely robust, can only be dissolved in strong acids such as trifluoroacetic acid (TFA), and have a regular rodlet morphology.<sup>7</sup> Class II hydrophobins form assemblies that lack a distinct rodlet morphology and can be dissolved in detergent and alcohol solutions.<sup>8</sup> Curiously, despite these clear sequence and morphological differences, no obvious distinction between the functions of class I and class II hydrophobins within the fungal life cycle has yet emerged.

Class II hydrophobins are generally smaller than class I proteins (~70 residues *versus* ~85–95 residues) and display substantially more sequence similarity to one another<sup>1</sup> (Fig. 1a). The length of the polypeptide segments between cysteines 3 and 4 (the Cys3–Cys4 loop) and that between cysteines 4 and 5 (the Cys4–Cys5 loop) are fully conserved in class II hydrophobins, and the other inter-cysteine regions are also well conserved. In contrast, class I hydrophobins display much greater sequence variation. In particular, the length of the inter-cysteine regions is highly variable. The Cys3–Cys4 loop varies from 4 residues (HYD3 from *Gibberella moniliformis*) to 44 residues (AaPRI2 from *Agrocybe aegerita*), and the Cys4–Cys5 loop varies from 8 residues (EAS from *Neurospora crassa*) to 23 residues (DewA from *Aspergillus nidulans*). Across the entire

hydrophobin family, the N-termini vary in sequence and length and do not appear to be critical for the structural integrity of the proteins or their surface activity.<sup>1</sup>

Despite the very low level of sequence conservation, class I and class II hydrophobins share very similar folds. The crystal structures of two highly homologous class II hydrophobins, HFBI and HFBII, from *Trichoderma reesei* have been solved by X-ray crystallography,<sup>9–12</sup> and the solution structure of EAS, a class I hydrophobin from *N. crassa*, has been determined using triple-resonance NMR methods.<sup>13</sup> All three structures have almost identical  $\beta$ -barrel folds that are composed of four antiparallel  $\beta$ -strands. Two of the four disulfides span the ends of the barrel, while the N-terminus is linked to the barrel through one disulfide; the last disulfide links either a small  $\alpha$ -helix (in HFBI and HFBII) or a two-stranded  $\beta$ -sheet (in EAS) to the outside of the barrel.

All three structures display an amphipathic character. In EAS, only 8 of the 82 residues are charged, and 6 of these are located on a single face of the protein,<sup>13</sup> giving rise to distinct hydrophilic and hydrophobic faces. On the other hand, the charged residues in HFBI and HFBII are more evenly distributed over the surface and the proteins do not display such a prominent charge separation. However, a large exposed hydrophobic patch is present in all three structures, and this presumably underlies the ability of hydrophobins to form amphipathic monolayers.

The most striking difference between the class I and class II hydrophobin structures is the pre-

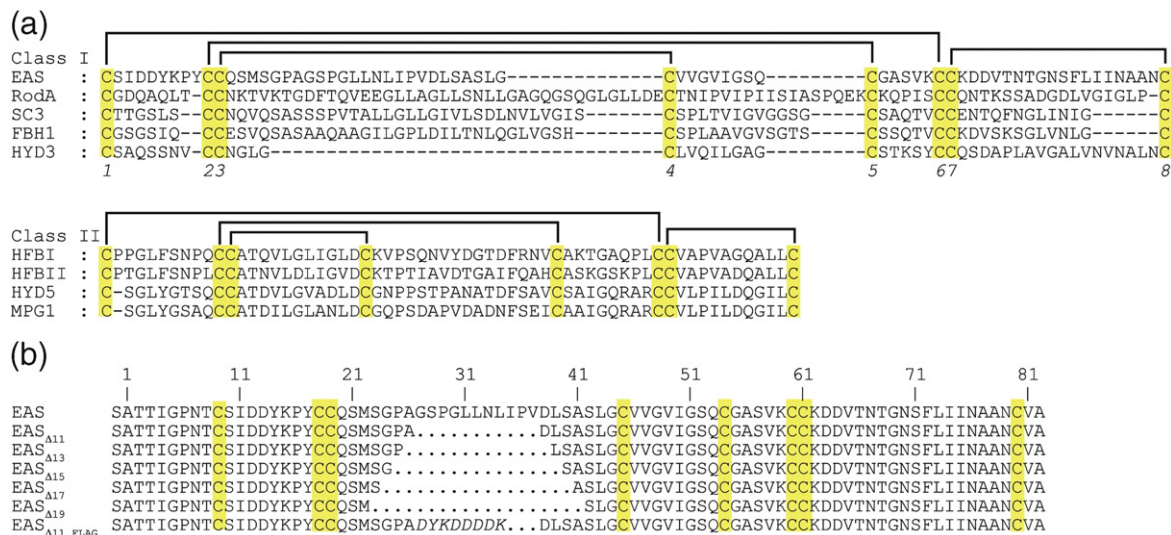


**Fig. 1.** Sequences of a representative subset of class I and class II hydrophobins and the EAS variants used in this study. (a) Amino acid sequence comparison of class I and class II hydrophobins. Only amino acids between the first and last Cys residues are shown due to high sequence variation outside this region. The conserved Cys residues are highlighted in yellow, with the conserved disulfide bonding pattern indicated with brackets. The hydrophobins used are as follows: EAS from *N. crassa* (accession code Q04571), RodA from *Aspergillus fumigatus* (accession code P41746), SC3 from *Schizophyllum commune* (accession code P16933), FBH1 from *Pleurotus ostreatus* (accession code O60047), HYD3 from *G. moniliformis* (accession code Q6YF30), HFBI from *T. reesei* (accession code P52754), HFBII from *T. reesei* (accession code P79073), HYD5 from *G. moniliformis* (accession code Q6YD93), and MPG1 from *Magnaporthe grisea* (accession code O94196). The cysteine numbering is indicated in italics below the sequences. (b) Sequences of the EAS variants constructed in this work. Residues deleted are indicated as dots, and residue numbers for full-length EAS are shown above the sequences. The FLAG-tag sequence is shown in italics.

sence of two disordered loops on the surface of the former—the Cys3–Cys4 and Cys7–Cys8 loops.<sup>13,14</sup> The 25-residue Cys3–Cys4 loop in EAS is extremely hydrophobic, whereas the smaller Cys7–Cys8 loop is made up predominantly of uncharged polar residues. It has been proposed that the Cys3–Cys4 loop in the class I hydrophobin SC3 is a major driver of rodlet assembly.<sup>15,16</sup> Assembly of SC3 into rodlets at an air–water interface involves the conversion of an  $\alpha$ -helical intermediate to a final form that is rich in  $\beta$ -sheet and that converts to rodlets over time. Protease digestion, hydrogen–deuterium exchange, and peptide studies suggest that the conformational changes may be initiated within the Cys3–Cys4 loop, which is presumed to adopt a helical structure when it initially adheres to a hydrophobic surface.<sup>16</sup>

We previously proposed two models for EAS rodlet assembly, one in which both the loops and the ordered  $\beta$ -barrel of the EAS monomer are incorporated into the regular rodlet structure and another in which only the ordered  $\beta$ -barrel is involved, leaving the disordered loops on the hydrophobic surface.<sup>13</sup> Both models are compatible with the observed amphipathic nature of the rodlets.

The variations in the length and the sequence of the loops in class I hydrophobins led us to undertake a study of the role of the Cys3–Cys4 loop in EAS, with a view to understanding its contribution to rodlet assembly, structure, and function. We show here that most of the Cys3–Cys4 loop can be deleted without affecting either the fold or physical properties of the monomeric protein or the morphology of the rodlets. Molecular dynamics simulations show that the deletion of the Cys3–Cys4 loop results in EAS binding to an air–water interface in a more ordered manner compared with the wild-type protein. Taken together, these results indicate that the residues in the Cys3–Cys4 loop of EAS are not involved in the initiation of rodlet assembly and are not required for formation of the rodlet scaffold. Rather, this loop may be involved in the lateral packing of rodlets to form a monolayer or might play a role in the interaction of *N. crassa* EAS rodlets with individual target surfaces.

## Results

### The EAS structure is tolerant of truncation of the Cys3–Cys4 loop

We previously reported that 11 residues could be removed from the Cys3–Cys4 loop without affecting the structure of EAS.<sup>13</sup> In order to examine the requirement for this loop in more detail, we systematically removed 13, 15, 17, 19, and 21 residues from the Cys3–Cys4 loop. Each of the variants (herein known as EAS $_{\Delta 13}$ , EAS $_{\Delta 15}$ , EAS $_{\Delta 17}$ , EAS $_{\Delta 19}$ , and EAS $_{\Delta 21}$ , respectively) was overexpressed, refolded, and purified as described for wild-type EAS.<sup>13</sup> Mutants lacking 13, 15, or 17 residues folded normally; indeed, the removal of up to 15 amino acids

from the Cys3–Cys4 loop *enhances* the efficiency of the refolding of the proteins, as judged by the fraction of protein that could be correctly refolded during purification. Correctly folded protein could be separated from unfolded and incorrectly folded species by reversed-phase HPLC (rpHPLC). Refolding efficiency was therefore judged by the size and shape of the protein peaks on the rpHPLC trace and the characteristics of the NMR spectra. In contrast, the removal of 19 or more residues disrupted the EAS structure: neither EAS $_{\Delta 19}$  nor EAS $_{\Delta 21}$  could be refolded successfully; each formed multiple species on rpHPLC (data not shown). Further characterization of these two mutants was not pursued.

One-dimensional (1D) <sup>1</sup>H NMR spectra collected on the remaining EAS mutants showed that they are generally well folded and monomeric (Fig. 2a). Both chemical shift dispersion and linewidths in these spectra are comparable with those in the wild-type EAS spectrum. Also, the positions of highly shifted signals in all mutants are preserved, suggesting that there has been little perturbation of the overall EAS fold. As expected, the number of NMR signals arising from the unfolded regions of the protein decreased, because up to 15 residues had been removed from the flexible loop. The 1D NMR spectrum of EAS $_{\Delta 17}$ , however, shows the presence of additional signals with chemical shifts characteristic of unfolded polypeptide (among signals arising from folded regions of the protein). The rpHPLC trace of EAS $_{\Delta 17}$  displays a broad peak with significant shoulder regions (not shown), and it is therefore likely that the NMR sample contains a mixture of correctly folded EAS $_{\Delta 17}$  and misfolded and/or incompletely folded proteins. Overall, the data indicate that up to 17 residues can be removed from the large loop of EAS without affecting the EAS fold.

### The structure of monomeric EAS $_{\Delta 15}$ closely resembles that of full-length EAS

A detailed structural and biophysical analysis of EAS $_{\Delta 15}$  was undertaken in order to determine whether the removal of residues from the Cys3–Cys4 loop affected the structure and function of EAS monomers. This EAS $_{\Delta 15}$  mutant was chosen because of the high quality of its 1D <sup>1</sup>H NMR spectrum. The 3D structure of the EAS $_{\Delta 15}$  mutant was determined using standard <sup>1</sup>H/<sup>15</sup>N NMR methods as described previously.<sup>13,17</sup> The 20 lowest-energy structures from the final ARIA calculations were chosen to represent the solution structure of EAS $_{\Delta 15}$  (Fig. 3a and b; Table 1). Overlays of EAS $_{\Delta 15}$  with full-length EAS (Fig. 3c) and the class II hydrophobin HFBI (Fig. 3d) show that the core  $\beta$ -barrel structure is conserved in EAS $_{\Delta 15}$ . The EAS $_{\Delta 15}$  structure lacks the long disordered region seen in EAS, and in its place is a short six-residue turn. This turn links two strands in the  $\beta$ -hairpin that forms part of the core. Inspection of the structure suggests that there is little scope for further substantial shortening of the loop, consistent with our observations on EAS $_{\Delta 19}$  and EAS $_{\Delta 21}$ . Importantly, the removal of the long hydro-

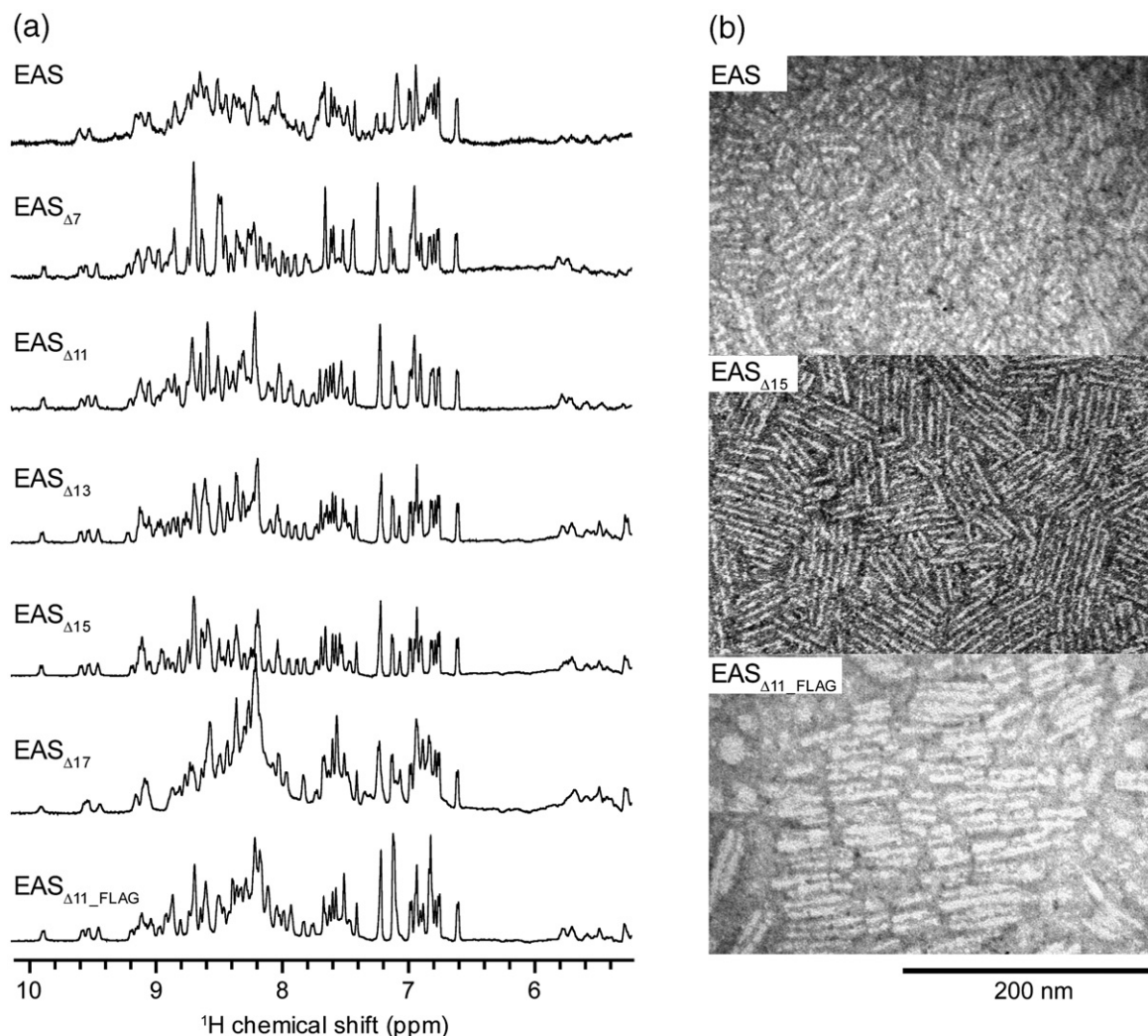


**Fig. 2.** Analysis of EAS mutants. (a) One-dimensional  $^1\text{H}$  NMR spectra showing the amide region of wild-type EAS and mutants. All proteins were resuspended in 20 mM sodium acetate with 5%  $\text{D}_2\text{O}$ , pH 6.2, or 20 mM sodium phosphate with 5%  $\text{D}_2\text{O}$ , pH 6.2. All spectra were recorded at 298 K. (b) Transmission electron micrographs of EAS proteins. EAS,  $\text{EAS}_{\Delta 15}$ , and  $\text{EAS}_{\Delta 11\_FLAG}$  are shown in the top, middle, and bottom panels, respectively.

phobic loop does not change the high amphipathicity exhibited by the core region of the molecule: the six charged residues clustered on a single surface on full-length EAS are positioned similarly in  $\text{EAS}_{\Delta 15}$ .

In order to test the structural resilience of EAS and  $\text{EAS}_{\Delta 15}$ , we carried out molecular dynamics simulations of the proteins in water. Panels (f) and (g) in Fig. 3 show a superimposition of 20 frames from a 10-ns simulation of EAS and that of  $\text{EAS}_{\Delta 15}$ , respectively. As can be seen in the figures, the core  $\beta$ -barrel structures of both EAS and  $\text{EAS}_{\Delta 15}$  are highly stable in the simulations. In contrast, the Cys3–Cys4 region (the long loop), the Cys7–Cys8 region, and the termini show considerable flexibility, consistent with the lack of nuclear Overhauser enhancements (NOEs) from these regions.<sup>13</sup>

#### Truncation mutants are capable of forming rodlets

EAS truncation mutants with up to 17 residues removed are capable of forming native-like rodlets

(Fig. 2b and other data not shown). EAS and  $\text{EAS}_{\Delta 15}$  rodlets are highly robust and are insoluble in a range of buffers and conditions (including 70% ethanol, 10% SDS, and 8 M urea) but can be resolubilized by neat TFA (data not shown). This is one of the defining features of class I hydrophobin rodlets, and, overall, the properties of the rodlets formed from the truncation mutants are indistinguishable from those of wild-type EAS. This result indicates that the Cys3–Cys4 loop is not required for rodlet formation and that residues in the loop are not responsible for the unusual robustness of hydrophobin rodlets.

#### $\text{EAS}_{\Delta 15}$ is highly surface active

High surface activity is a characteristic feature of the hydrophobins and forms the basis of the many biotechnology applications that have been suggested for these proteins.<sup>18,19</sup> The structure of  $\text{EAS}_{\Delta 15}$  reveals that the unique charge distribution observed in the core region of wild-type EAS is maintained and suggests that  $\text{EAS}_{\Delta 15}$  should be surface active,

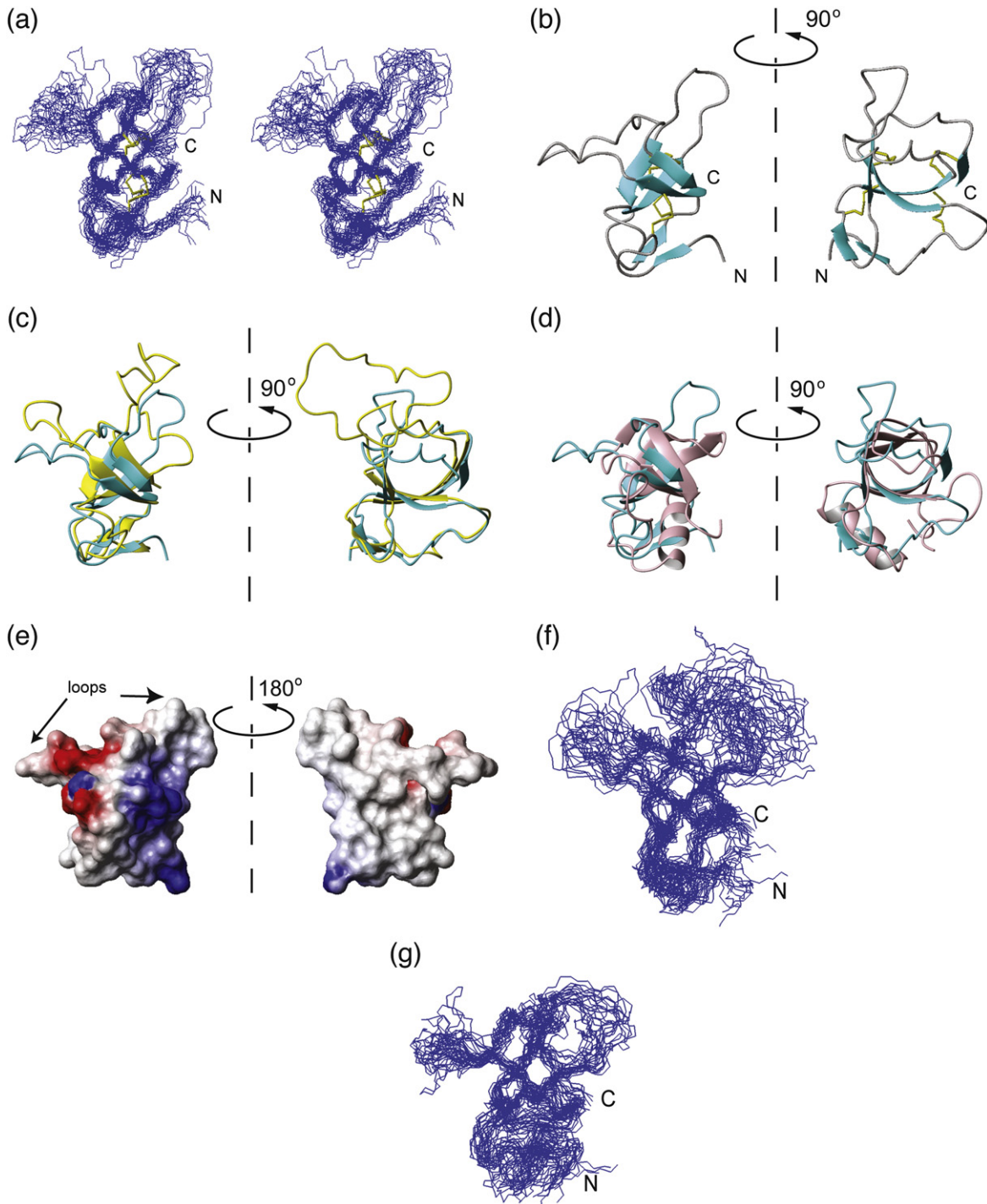


**Fig. 3.** Solution structure of EAS $_{\Delta 15}$ . (a) Overlay of the 20 lowest-energy conformers of EAS $_{\Delta 15}$  shown in stereoview. (b) Ribbon diagram of EAS $_{\Delta 15}$ . Disulfide bonds and Cys side chains are shown as yellow sticks. (c) Overlay of EAS $_{\Delta 15}$  with full-length EAS. The lowest-energy structure of EAS $_{\Delta 15}$  is shown in cyan, and that of full-length EAS (PDB ID code 2FMC) is shown in yellow. (d) Overlay of EAS $_{\Delta 15}$  with the X-ray crystal structure of HFBII. The lowest-energy structure of EAS $_{\Delta 15}$  is shown in cyan, and HFBII (PDB ID code 1R2M) is shown in pink. (e) Electrostatic surface of EAS $_{\Delta 15}$ . Positive and negative charges are shown in blue and red, respectively. It is clear that almost all charged residues lie on a single face of the protein. (f) Superposition of 20 structures sampled every 0.5 ns from a 10-ns simulation of EAS in water. (g) Superposition of 20 structures sampled every 0.5 ns from a 10-ns simulation of EAS $_{\Delta 15}$  in water.

although it is not clear whether the long hydrophobic loop in EAS contributes to the high surface activity of the protein. We used contact angle measurements to assess the surface activity of EAS $_{\Delta 15}$  rodlets com-

pared with wild-type EAS. The contact angles formed by aqueous drops containing equal molar concentrations of either wild-type EAS or EAS $_{\Delta 15}$  on a Teflon<sup>®</sup>-coated slide were determined using a DSA10<sub>MK2</sub>

**Table 1.** Structural statistics for EAS $_{\Delta 15}$ 

<i>Experimental input</i>	
Total NOE restraints	1407
Total unambiguous restraints	1236
Intraresidue	559
Sequential	323
Medium range (2–4 residues)	74
Long range ( $\geq 5$ residues)	280
Total ambiguous restraints	171
Disulfide bond restraints (between residues 9 and 45, 18 and 39, 19 and 30, 46 and 65)	4
Torsion angle constraints (dihedral $\phi$ )	31
<i>Quality control</i>	
PROCHECK statistics (residues 2–5, 13–20, 27–48, and 57–66) <sup>a</sup>	
Residues in most favored regions	72.4%
Residues in allowed regions	23.2%
Residues in generously allowed regions	2.4%
Residues in disallowed regions	2.1%
<i>RMSDs</i>	
Backbone atoms	
2–5, 13–20, 27–48, 57–66	0.82 $\pm$ 0.13
2–20, 27–48, 57–66	0.89 $\pm$ 0.14
All heavy atoms	
2–5, 13–20, 27–48, 57–66	1.15 $\pm$ 0.11
2–20, 27–48, 57–66	1.23 $\pm$ 0.11
<i>Mean deviations from ideal geometry</i>	
Bond lengths	0.0035 $\pm$ 0.0001 Å
Bond angles	0.42 $^{\circ}$ $\pm$ 0.02 $^{\circ}$

<sup>a</sup> Note that residues 2–5, 13–20, 27–48, and 57–66 correspond to residues 2–5, 13–20, 42–63, and 72–81 in full-length EAS.

system (KRUSS, Hamburg, Germany). Both proteins are highly surface active and are able to reduce measurably the contact angle formed by water on a hydrophobic surface (Fig. 4a). These measurements indicated that EAS $_{\Delta 15}$  might be slightly less surface active than wild-type EAS at the same molar concentration (with a contact angle of 80.4 $^{\circ}$  $\pm$ 10.1 $^{\circ}$  for EAS $_{\Delta 15}$  and that of 73.7 $^{\circ}$  $\pm$ 11.7 $^{\circ}$  for EAS;  $p=0.067$  using two-tailed Student's  $t$  test). However, when using equal concentrations by mass, the activity of EAS $_{\Delta 15}$  is similar to that of wild-type EAS. Therefore, the removal of the long loop from EAS does not significantly affect the surface activity of the protein and the high surface activity of EAS must arise predominantly from the amphipathic nature of its core region.

### EAS $_{\Delta 15}$ forms native-like rodlets with structural properties similar to EAS rodlets

EAS $_{\Delta 15}$  is observed to form native-like rodlets under electron microscopy (Fig. 2b). Circular dichroism (CD) spectropolarimetry was used to compare the secondary structure contents of EAS $_{\Delta 15}$  and EAS rodlets. Samples of EAS $_{\Delta 15}$  and EAS were applied to one face of a quartz cuvette and allowed to dry overnight. CD spectra of solution and dried-down EAS $_{\Delta 15}$  and EAS are shown in Fig. 4b. The spectra from the monomeric forms of the proteins are dominated by contributions from coil regions (minimum at  $\sim 195$  nm); the small  $\beta$ -barrel structure does

not give rise to a strong  $\beta$ -signal. Upon drying, the minima are shifted to  $\sim 210$  and  $\sim 220$  nm for EAS $_{\Delta 15}$  and EAS, respectively. These spectra are comparable with those observed previously for oriented  $\beta$ -sheet films<sup>20,21</sup> and indicate that regularization or extension of the existing  $\beta$ -structure must occur upon rodlet assembly. It is not clear why the positions of the minima differ between wild-type EAS and EAS $_{\Delta 15}$ : it is possible that the long loop adopts additional  $\beta$ -sheet structures in the rodlet form, thus resulting in the larger shift observed for rodlets composed of full-length EAS.

### EAS $_{\Delta 15}$ assembles into rodlets with kinetics similar to those for wild-type EAS

The aromatic dye thioflavin T (ThT) binds specifically to stacked  $\beta$ -sheet structures, an interaction that results in a dramatic increase in the fluorescence emitted by the dye at 485 nm. For this reason, ThT has been used extensively to monitor amyloid formation in solution.<sup>22</sup> Hydrophobin rodlets share many structural similarities with amyloid fibers, and the rodlets from the class I hydrophobin SC3

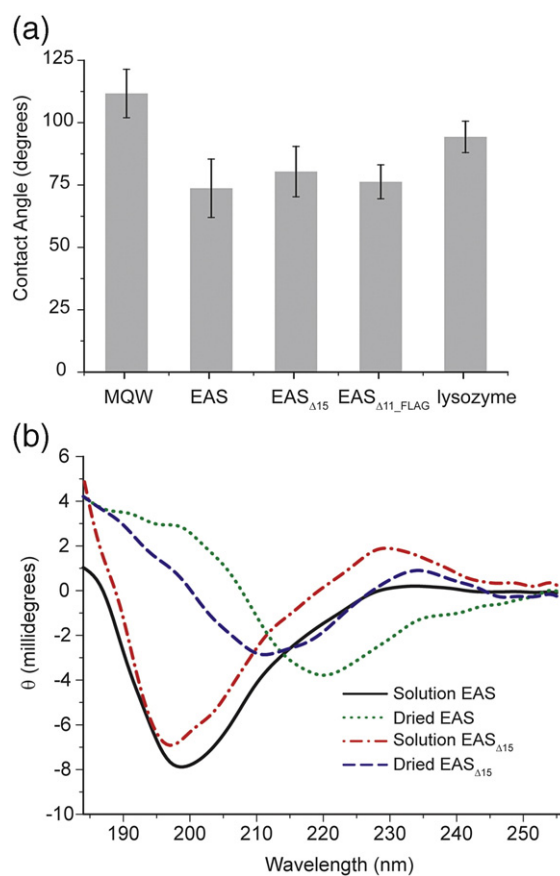


**Fig. 4.** (a) Average contact angles of 4- $\mu$ L drops on Teflon<sup>®</sup>-coated slides. Drop solutions contained 60  $\mu$ M EAS, EAS $_{\Delta 15}$ , EAS $_{\Delta 11\_FLAG}$ , lysozyme, or water only. Error bars shown are 1 SD from the mean of 16–18 measurements. (b) CD spectra of EAS and EAS $_{\Delta 15}$  in water and dried onto a quartz cuvette.

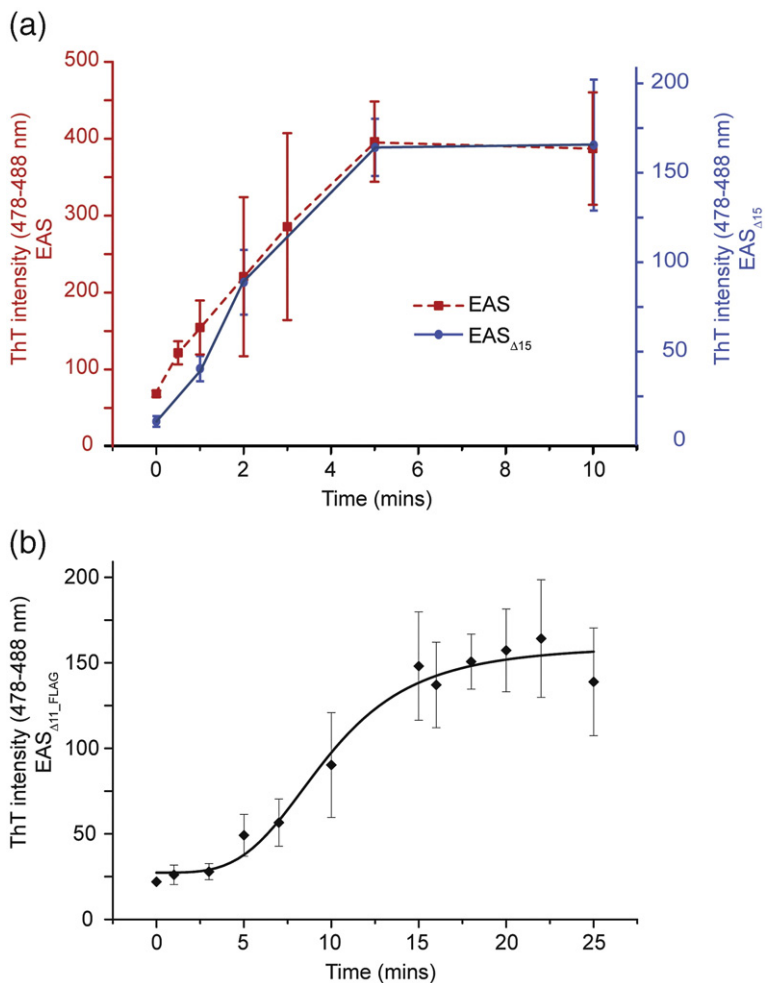


**Fig. 5.** Time course for rodlet formation as monitored by ThT binding. Solutions containing 10  $\mu$ M EAS proteins and 37.5  $\mu$ M ThT were vortexed at high speed for varying lengths of time. Error bars shown are 1 SD from the mean of eight replicates. Lines are drawn only to guide the eye. Time courses for (a) EAS and EAS $_{\Delta 15}$  and (b) EAS $_{\Delta 11\_FLAG}$  are shown. Note that different scales for EAS and EAS $_{\Delta 15}$  are shown to highlight the similarity in the kinetics of rodlet formation.

have been shown to bind ThT.<sup>23</sup> Figure 5a shows an increase in ThT fluorescence at 485 nm as a function of vortexing time when an EAS-containing solution was induced to form rodlets by vigorous vortexing, a process that maximizes the air–water interfaces within the sample. The increase in ThT fluorescence with the extent of vortexing was used to monitor the rate of rodlet formation by EAS and EAS $_{\Delta 15}$ . The fluorescence signals from ThT mixed with both EAS and EAS $_{\Delta 15}$  increased with increasing vortexing time and reached a maximum after approximately 5 min, suggesting that all of the monomeric form of the protein had been converted into the rodlet state by this time. The observation that EAS and EAS $_{\Delta 15}$  display similar kinetics of rodlet formation reinforces the view that the large flexible loop of EAS is not responsible for driving hydrophobin assembly.

#### EAS $_{\Delta 15}$ binds specifically to air–water interface in molecular dynamics simulations

Previous simulation studies of a structurally related hydrophobin (SC3) suggested that the protein bound to an air–water interface via the Cys3–Cys4 loop.<sup>15</sup> However, a range of experimental observations indicate that the binding properties of EAS $_{\Delta 15}$

are very similar to those of full-length EAS, despite the fact that the majority of the Cys3–Cys4 loop has been removed. To study the binding of full-length EAS and EAS $_{\Delta 15}$  to an air–water interface in near-atomic detail, we performed a series of molecular dynamics simulations in which a single copy of EAS or EAS $_{\Delta 15}$  was placed in the middle of a box of water near an air–water interface in a random orientation and allowed the system to evolve over time. As found previously with SC3, both EAS and EAS $_{\Delta 15}$  bound spontaneously to the air–water interface and, once bound, did not detach during the entire length of the simulations (up to 30 ns). Snapshots from a trajectory illustrating a typical sequence of events during the binding of full-length EAS to an air–water interface are shown in Fig. 6. Starting in the middle of the box, the protein can be seen to rotate freely before binding to the interface, demonstrating that the binding orientation is not determined by the starting configuration. Although conformations in which the Cys3–Cys4 loop is close to the interface are found during the simulations (data not shown), this loop does not appear to play a direct role in the binding to the interface.

Following initial binding, the system relaxes over time such that the core of the protein is in contact with the interface and only a small part of the loop is

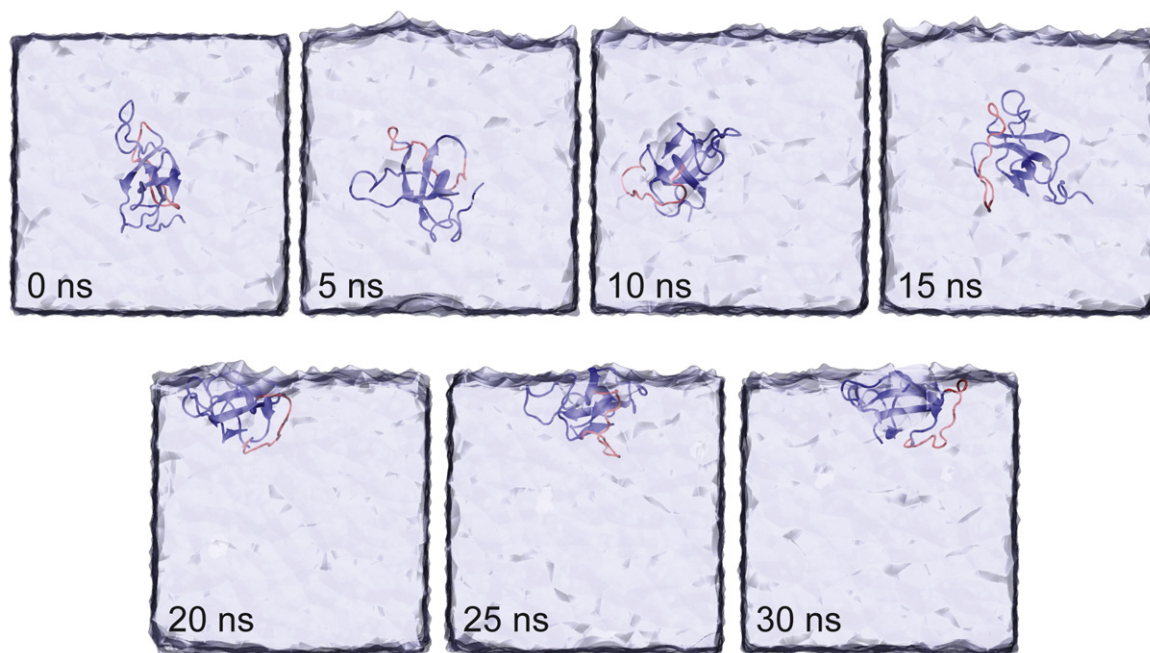


**Fig. 6.** Snapshots taken every 5 ns from a 30-ns simulation of full-length EAS interacting with an air–water interface (upper and lower faces of the box). The EAS protein is shown in cartoon representation. Residues 25–39, those removed to generate EAS $_{\Delta 15}$ , are shown in red, while the rest of the protein is shown in blue.

involved. Figure 7a shows the relative positions of the C $^{\alpha}$  atoms of EAS and EAS $_{\Delta 15}$  along the z-axis averaged over the last 5 ns of each 30-ns simulation. As can be seen from Fig. 7a, EAS does not adopt a well-defined orientation with respect to air–water interfaces on the time scale of the simulations. In particular, there is no specific preference for the Cys3–Cys4 loop to interact either with the interface or with the water. In addition, while regions of the protein close to residues 55 and 70 clearly project toward the interface, it is not possible to identify specific residues that consistently bind to the interface. In contrast, it can be seen that irrespective of its starting position, EAS $_{\Delta 15}$  binds to the air–water interface in the same orientation (Fig. 7a). In particular, certain sets of residues, namely, residues 3–8 (TIGPNT), 11–16 (IDYKYP), 46–54 (VVGVIQSQC), and 65–70 (VTNTGN), are consistently found interacting with the interface (Fig. 7b). Interestingly, these surfaces contain several polar and charged residues. While it is not possible to directly relate the differences in binding seen in the simulations on a nanosecond time scale to the macroscopic properties of the system, the fact that EAS $_{\Delta 15}$  binds to the air–water interface in a much more regular fashion than native EAS might explain the enhanced degree of order we observe in our electron microscopic images of EAS $_{\Delta 15}$  rodlets.

#### Introduction of the highly charged FLAG sequence into the flexible loop affects rodlet assembly

Given that most of the Cys3–Cys4 loop is not required for the structure and function of EAS, the

effect of the loop sequence was tested by substituting the original predominantly hydrophobic loop with the short but highly charged FLAG sequence (DYKDDDDK).

The FLAG sequence was inserted into EAS $_{\Delta 11}$  (to create EAS $_{\Delta 11\_FLAG}$ ), and this variant was over-expressed, refolded, and purified as described for EAS and the truncation variants. A 1D  $^1\text{H}$  NMR spectrum showed that EAS $_{\Delta 11\_FLAG}$  is well folded and monomeric, with chemical shift dispersion and linewidths comparable with those observed for wild-type EAS (Fig. 2a). Surprisingly, despite the addition of seven charges to the protein, the ability of EAS $_{\Delta 11\_FLAG}$  to lower the contact angle formed by aqueous drops on a Teflon $^{\text{®}}$ -coated slide was similar to that of EAS and that of EAS $_{\Delta 15}$  (Fig. 4a). This further supports the idea that the surface activity of EAS arises primarily from the unique separation of charges in the core region of the protein.

Observation of EAS $_{\Delta 11\_FLAG}$  rodlets by transmission electron microscopy suggests that this variant forms structures with a somewhat altered morphology relative to the wild-type rodlets (Fig. 2b). In particular, the EAS $_{\Delta 11\_FLAG}$  rodlets appear to be wider (widths of the EAS, EAS $_{\Delta 15}$ , and EAS $_{\Delta 11\_FLAG}$  rodlets are  $7.1 \pm 1.2$ ,  $6.1 \pm 0.4$ , and  $8.5 \pm 0.7$  Å, respectively), more irregular, more paired, and less well packed. Like EAS rodlets, however, EAS $_{\Delta 11\_FLAG}$  rodlets are also insoluble in 70% ethanol, 10% SDS, and 8 M urea but can be solubilized by neat TFA.

The FLAG-tag insertion also slows the kinetics of rodlet assembly. The ThT fluorescence signal from an EAS $_{\Delta 11\_FLAG}$  solution was monitored at 485 nm with increasing vortexing time (Fig. 5b), and this was observed to reach its maximum value after 20–

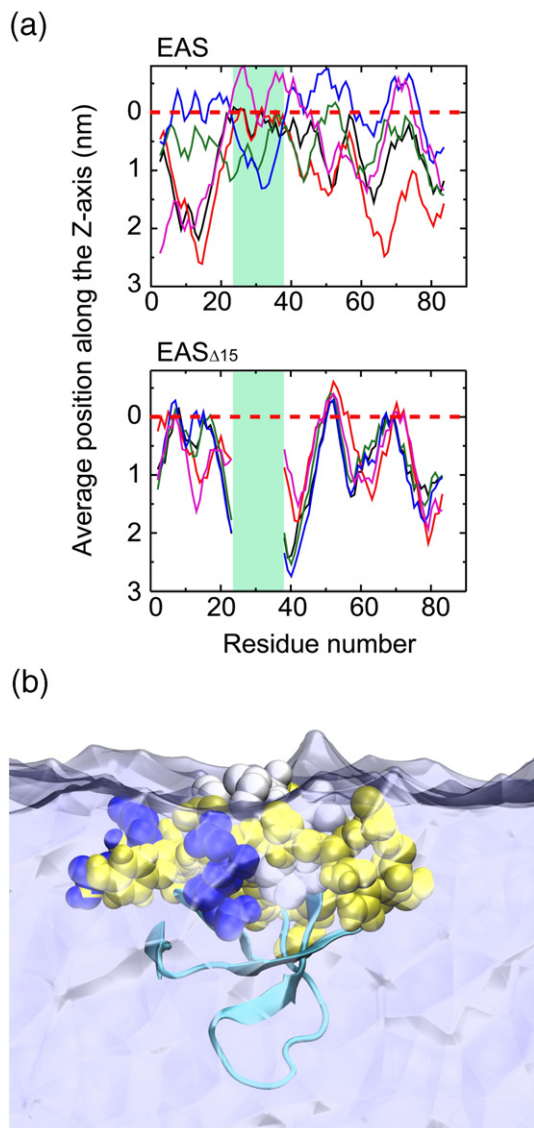


**Fig. 7.** The orientation of EAS and EAS $\Delta_{15}$  at an air-water interface. (a) The average position of the C $\alpha$  atoms of EAS (upper) and EAS $\Delta_{15}$  (lower) with respect to the air-water interface along the z-axis (normal to the air-water interface). The average is calculated over the last 5 ns of each 30-ns simulation. The five colored lines represent independent simulations starting from different initial conditions (see Materials and Methods). The air-water interface is represented by the red dashed line ( $z=0$ ). Residues 25–39, which are not present in EAS $\Delta_{15}$ , are indicated by the green shaded area. Residue numbering corresponds to full-length EAS. (b) A representative conformation of EAS $\Delta_{15}$  interacting with an air-water interface. Residues that on average lie within 0.5 nm of the air-water interfaces as indicated in (a) are drawn as space-filling models (polar, yellow; hydrophobic, white; Asp, blue).

25 min of vortexing in contrast to EAS and EAS $\Delta_{15}$ , which reached a maximum after 5 min. Furthermore, a short lag phase in the buildup of fluorescence is observed, suggesting that the insertion of the charges slows the rate at which monomers polymerize into rodlets.

## Discussion

### The long loop of EAS and its role in hydrophobin assembly

Most class I hydrophobins have a long loop of at least 18 residues between Cys3 and Cys4. The proposed 3D model of the hydrophobin SC3, the only other class I hydrophobin for which extensive structural and biophysical data are available, indicates that the Cys3–Cys4 loop is highly flexible.<sup>15,16</sup> In molecular dynamics simulations of SC3, the center part of this loop preferentially binds interfaces;<sup>15</sup> it has also been demonstrated experimentally that this long loop binds strongly to colloidal Teflon and, upon doing so, becomes more protected from hydrogen–deuterium exchange.<sup>24</sup> These results, along with evidence from limited proteolysis experiments, have led to the idea that the Cys3–Cys4 loop is pivotal to hydrophobin self-assembly.

Here, we show that it is possible to remove up to 17 amino acids from the middle of the 25-residue loop of EAS (leaving only 8 residues, even fewer than in class II proteins) and still generate rodlets with typical class I properties, including a clear rodlet morphology under electron microscopy and the inability to be solubilized by 70% ethanol and 10% SDS. Furthermore, the kinetics of rodlet formation (at least up to the stage of formation of  $\beta$ -sheet stacks) are unaffected by reducing the length of the loop, as judged by ThT binding. This suggests that the flexible loop neither drives the interaction of EAS monomers with the interface nor promotes polymerization of monomers once they are there. This finding is consistent with our contact angle measurements that show EAS $\Delta_{15}$  and EAS having a similar surface activity. It appears that the major determinant of surface activity and thereby rodlet assembly at interfaces is the amphipathic nature of the core region of EAS, with the long and flexible Cys3–Cys4 loop playing a minor role, if any. This would explain why class I hydrophobins with such variations in length and amino acid composition, especially in the loop regions (with sequence identity as low as <10% between some members), can share the same core structure and can polymerize into rodlets with similar morphology and dimensions. However, removal of >17 residues from the Cys3–Cys4 loop resulted in the inability of the truncated EAS to refold under standard conditions. It is possible that the remaining loop residues do play a role in rodlet assembly in the EAS proteins.

Although the EAS $\Delta_{15}$  variant is more like class II hydrophobins in that it has a shorter and relatively structured Cys3–Cys4 loop, it still clearly retains the ability to form ordered and robust rodlets. Therefore, differences other than the length of the Cys3–Cys4 loop, such as having a more defined overall structure and having a less pronounced separation of charged and hydrophobic surface residues, may account for the lack of rodlet morphology and the less robust nature of the class II assemblies. Further

work will be required to identify the key structural regions that define the two classes.

### Conformation adopted by the long loop in assembled rodlets

CD studies performed using soluble and polymerized EAS and EAS $_{\Delta 15}$ , together with CD and attenuated total reflectance Fourier-transform infrared data from rodlets formed by other class I hydrophobins,<sup>25,26</sup> suggest that there is a substantial increase in  $\beta$ -structure upon polymerization. It is notable that this increase in  $\beta$ -structure is also observed with the EAS $_{\Delta 15}$  mutant despite the drastic reduction in the length of the flexible region. The observed increase in  $\beta$ -structure is therefore likely to result from the regularization or extension of the existing core  $\beta$ -structure upon rodlet assembly through intermolecular hydrogen bonding between  $\beta$ -strands. While the data suggest that the Cys3–Cys4 loop may contribute additional oriented  $\beta$ -sheet structural elements to the rodlets, these additional structural elements do not appear to be required for EAS assembly or for the unique properties of hydrophobins but may rather be a consequence of rodlet formation.

### Model of rodlet assembly

We previously proposed two possible models for the arrangement of EAS monomers in the rodlets.<sup>13</sup> In both models, the  $\beta$ -barrel core of EAS was arranged in a head-to-tail fashion along the rodlets, with hydrogen bonds formed between the exposed strands of adjacent monomers. The amphipathic nature of the rodlets at the interface results from mutual alignment of the hydrophilic and hydrophobic faces of the EAS monomers. In one model, the Cys3–Cys4 loop was incorporated into the structure in a way that extended the  $\beta$ -barrel core, whereas in the other, the loop was not involved in rodlet formation. The results reported here are more consistent with the latter model, in which the monomers stack along the long axis of the rodlet, forming backbone hydrogen bonds between the trailing/leading edges of adjacent  $\beta$ -barrel cores. This model would predict the average length of the rodlets to be the same irrespective of the length of the loop, provided the same number of monomers is stacked together. From the current studies, it appears that EAS and the various truncation mutants do form rodlets with similar lengths. However, it should be noted that the morphology of the rodlets does depend to some extent on the exact experimental conditions.

A model based on a direct interaction between the core regions of successive monomers would also explain why an EAS mutant with substantial modification of the loop (e.g., EAS $_{\Delta 11\_FLAG}$ ) could still form rodlets, as well as why the rates of rodlet formation are essentially the same in EAS and EAS $_{\Delta 15}$ . Interestingly, the rodlets formed by EAS $_{\Delta 11\_FLAG}$  do appear to be wider than those formed by EAS and to

pack less tightly together than the full-length protein and its truncation variants, suggesting that the Cys3–Cys4 loop may be positioned between or around the individual rodlets and may affect their lateral packing. Since the FLAG tag is highly charged, it is possible that electrostatic repulsion between adjacent monomers, as well as between individual rodlets, might result in the observed alteration in rodlet morphology. This is consistent with our finding that the formation of stacked  $\beta$ -sheets in EAS $_{\Delta 11\_FLAG}$ , as detected by ThT binding assay, is substantially slower than that in EAS and its truncation mutants. Atomic force microscopy could be employed to determine whether the loop does play a role in mediating contact between adjacent rodlets, since the forces required to pull the rodlets apart would be expected to be different in EAS and its loop insertion and deletion variants.

### EAS is both functionally and structurally robust

Two of the most interesting features of class I hydrophobins are their high surface activity and their ability to self-assemble at interfaces to form an amphipathic rodlet layer that is highly robust. Many proposed applications of hydrophobins are ultimately tied to these two unique features. We have found that the monomeric EAS structure is tolerant of both truncation and insertion mutations in its long and flexible loop. Also, these mutations do not disrupt the ability of the protein to assemble into rodlets and do not significantly affect the surface activity of EAS. Moreover, the rodlets that are formed from the mutants are robust, with physicochemical properties similar to those of wild-type rodlets. This is very encouraging for the future design of hydrophobin-based molecules and suggests that functional groups might be incorporated into the flexible loop without affecting hydrophobin function and self-assembly.

## Materials and Methods

### Production of recombinant EAS and mutagenesis

All EAS truncation mutants were subcloned, over-expressed, and purified as described previously.<sup>13</sup> EAS $_{\Delta 13}$ , EAS $_{\Delta 15}$ , EAS $_{\Delta 17}$ , EAS $_{\Delta 19}$ , and EAS $_{\Delta 21}$  were constructed by deletion of residues 26–38, 25–39, 24–40, 23–41, and 22–42 inclusive from EAS, respectively. EAS $_{\Delta 11\_FLAG}$  was constructed by inserting the FLAG-tag sequence (DYKDDDDK) into the EAS $_{\Delta 11}$  background at the site of the truncation (Fig. 1b).

### NMR spectroscopy

NMR samples (0.1–0.5 mM, depending on the mutant used) were prepared as described previously.<sup>13</sup> All samples were made in 20 mM sodium acetate with 5% D<sub>2</sub>O, pH 6.2, or 20 mM sodium phosphate with 5% D<sub>2</sub>O, pH 6.2. Spectra were acquired at 298 K on an Avance 600-MHz NMR spectrometer (Bruker, Karlsruhe, Germany)

equipped with a triple-resonance cryoprobe, processed using Topspin 1.3 (Bruker), and analyzed using SPARKY†. The following spectra were acquired on EAS $_{\Delta 15}$ : double-quantum-filtered correlated spectroscopy, total correlation spectroscopy (mixing times = 35 and 70 ms), NOE spectroscopy (NOESY; mixing times = 50 and 150 ms),  $^{15}\text{N}$  heteronuclear single-quantum coherence, HNHA, HNHB, and  $^{15}\text{N}$ -separated NOESY. Assignments were made by using standard methodology. NOE-derived distance restraints were obtained from the 2D NOESY and 3D  $^{15}\text{N}$ -edited NOESY.  $\phi$  angle restraints based on the  $^3J_{\text{HNH}\alpha}$  coupling constants were measured from an HNHA.<sup>27</sup>

### Structure calculations

Structure calculations were carried out as reported previously<sup>13</sup> unless otherwise stated below. Because the  $^{15}\text{N}$  heteronuclear single-quantum coherence spectra from EAS and EAS $_{\Delta 15}$  overlay extremely well with each other (particularly over the Cys residues), the EAS $_{\Delta 15}$  mutant is assumed to have the same disulfide bonding pattern as EAS. Four disulfide bonds (between residues 19 and 30, 18 and 39, 9 and 45, as well as 46 and 65) were therefore incorporated into the calculations. The 100 lowest-energy structures from iteration 8 were refined in a 9-Å shell of water molecules, and the 20 conformers with the lowest value of  $E_{\text{tot}}$  were visualized and analyzed with the use of MOLMOL<sup>28</sup> and PROCHECK-NMR.<sup>29</sup>

### CD spectroscopy

CD spectra were recorded as reported previously.<sup>14</sup> Solution CD samples were made with lyophilized proteins in Milli-Q™ water (MQW) to a concentration of ~5  $\mu\text{M}$ . For solid-phase spectra, 10  $\mu\text{L}$  of EAS and EAS $_{\Delta 15}$  dissolved in MQW (to a concentration of ~60  $\mu\text{M}$ ) was spotted on the inside face of a horizontally placed quartz cuvette and allowed to air dry overnight. All data were baseline corrected by subtraction of a spectrum of MQW (for solution samples) or the cuvette alone (for dried samples).

### Contact angle measurements

To compare the surface activity of EAS and its mutants, we measured the contact angle formed by water droplets containing EAS and its mutants on a Teflon® surface. Drops of an aqueous solution of EAS or EAS mutants (4  $\mu\text{L}$ , 60  $\mu\text{M}$ ) were spotted onto a Teflon®-coated slide (Tekdon Incorporated, FL) that had been gently wiped with tissue to remove loose material. The slide was then tapped gently five times, while being kept horizontal, to encourage the drops to spread before being placed in a moist air-tight container until measured (~10 min after spotting). In our experience, tapping the slide reduced the variation in drop shape. In order to average the effects caused by the handling of each slide (e.g., during transport), we placed 3 drops of each of the four test samples (i.e., the proteins to be tested and a water control) on every slide. About 18 drops were measured in total for each protein (over six to eight slides). Profiles of the drops were digitized with a contour monitor at room temperature, and the contact angle was obtained using the drop shape analysis software running on the DSA10<sub>MK2</sub> system (KRUSS). These reported contact angle measurements are

not absolute since they do not take contact angle hysteresis into account; however, they allow a comparison of the relative surface properties of these proteins to be made.

### ThT binding assay

A stock ThT solution was prepared in MQW to a concentration of 4 mM and stored in aliquots at -20 °C until required. Prior to the start of the experiment, a fresh aliquot of ThT was thawed at room temperature and diluted with MQW to a working concentration of 45  $\mu\text{M}$ . EAS and mutant samples were prepared by dissolving lyophilized proteins in MQW to a concentration of 60  $\mu\text{M}$ . ThT working stock (250  $\mu\text{L}$ ) was first added to each well of a black fluorescence 96-well plate (Greiner, West Heidelberg, Victoria, Australia), and 50  $\mu\text{L}$  of EAS or an EAS mutant was then also added to the well. The samples were then sealed with SealPlate® (Excel Scientific, CA) and vortexed on a plastic platform at maximum setting for a predetermined time (see below for details). Once vortexing was completed, the plate was inverted once to mobilize bubbles that may have been stuck to the seal and then spun down briefly at 3000 rpm. The seal was removed carefully, and the samples in the plate were excited at 435 nm in a Varian Cary Eclipse fluorescence spectrophotometer (Varian Inc., CA). Fluorescence spectra were recorded over the wavelength range of 450–600 nm (with slit widths set at 10 nm for both excitation and emission). The experiments were staggered with respect to the end point of each experiment such that the cumulative vortexing times were reported in order to record all time points simultaneously using a single plate. For example, time points 0, 1, 2, and 5 min would be acquired by vortexing the first sample for 3 min, followed by addition of the second sample to the same plate and vortexing for 1 min, followed by the addition of the third sample and vortexing for another 1 min, and finally followed by the addition of the last sample. At this point, the plate would be centrifuged and read. Results shown are from eight replicates.

### Molecular dynamics simulations

A series of four systems was simulated. These were the full-length EAS and the truncated EAS $_{\Delta 15}$  in water and the full-length EAS and the truncated EAS $_{\Delta 15}$  at an air-water interface. A summary of the simulations performed is given in Table 2. The initial model for EAS was taken from Protein Data Bank (PDB) entry 2FMC,<sup>13</sup> and the structure of EAS $_{\Delta 15}$  was obtained as described above. In both cases, the first structure in the ensemble of NMR structures was taken. All acidic groups were protonated as appropriate at pH 2.0 to mimic low pH. Initially, the peptides were placed in a periodic box, solvated in water, and energy minimized. Each system was then simulated for 0.5 ns with the heavy atoms within the peptide positionally restrained using a harmonic force constant of

**Table 2.** Summary of the simulations of EAS and EAS $_{\Delta 15}$  peptides performed in water and in the presence of an air-water interface

System	Protein	Environment	No. of copies	Water molecules	Simulation length (ns)
1	EAS	Water	1	9116	10
2	EAS	Air-water	5	9116	30
3	EAS $_{\Delta 15}$	Water	1	6612	10
4	EAS $_{\Delta 15}$	Air-water	5	6612	30

† <http://www.cgl.ucsf.edu/home/sparky/>

1000 kJ mol<sup>-1</sup> nm<sup>-2</sup>. Each system was then simulated for 10 ns without restraints. From each of these simulations of EAS and EAS<sub>Δ15</sub> in water, five configurations were extracted (one every nanosecond from 1 to 5 ns) and used to initiate simulations of the peptides in the presence of an air–water interface (see Table 2). An air–water interface was created by extending the z-axis of the system by a factor of 2. In this way, the periodic system contained half vacuum. Each copy of the system was then again equilibrated for 0.1 ns with the protein positionally restrained. Finally, each copy was simulated for 30 ns without positional restraints.

All simulations were performed using version 3.3.1 of the GROMACS MD simulation package<sup>30</sup> in conjunction with the GROMOS53a6 force field.<sup>31</sup> The solvent water was modeled using the SPC water model. All simulations were performed under periodic boundary conditions. Bond lengths within the protein were constrained using the LINCS algorithm,<sup>32</sup> those within water, using SETTLE. The time step for integrating the equations of motion was 2 fs. The temperature was maintained by weak coupling to an external bath at 300 K, using a Berendsen thermostat with a coupling time of 0.1 ps. Systems simulated in the absence of an air–water interface (systems 1 and 3; Table 2) were simulated at a constant pressure. The pressure was maintained by coupling to a reference pressure of 1 bar with a coupling time of 10.0 ps, again using the method of Berendsen *et al.*<sup>33</sup> Simulations in the presence of an air–water interface were performed at constant volume. The nonbonded interactions were evaluated using a twin-range cutoff. Interactions within the short-range cutoff (0.9 nm) were updated every step, whereas interactions within the long-range cutoff (1.4 nm) were updated every five steps together with the pair list. A reaction field correction was used to correct for the truncation of long-range electrostatic interactions beyond the long-range cutoff.

### Electron microscopy

Fresh samples of EAS and EAS variants were prepared from lyophilized protein at a concentration of 0.1 mg/mL in 20% ethanol. Care was taken not to introduce air bubbles when the protein was dissolved. Drops of protein-containing solution (20 μL) were pipetted onto a sheet of Parafilm™ and allowed to stand for 10 min at room temperature. This allowed for the formation of a rodlet monolayer on the drop surface. Copper grids (200-μm mesh from ProSciTech, Australia) were prepared with pioloform plastic films and subsequently carbon coated. Protein was transferred by floating the grid on the surface of the protein-containing drop for 30 s. The excess liquid was removed by briefly touching the edge of the grid with filter paper. The grids were then washed by placing them briefly on a drop of water and then removing the water with filter paper as described above. Grids were stained by floating them on drops of 2% uranyl acetate for 10 min. Excess stain was removed by wicking with filter paper, and the grids were examined in a Phillips CM12 electron microscope operating at 120 kV, equipped with an iTEM digital imaging system, at the University of Sydney Electron Microscope Unit.

### Data deposition

The family of 20 lowest-energy structures has been deposited in the PDB‡ (PDB ID code 2k6a). NMR

assignment data have been deposited in the BioMagResBank§ (BioMagResBank ID code 15863).

### Acknowledgements

This work was supported in part by a Discovery Project Grant from the Australian Research Council (ARC; to M.S. and A.H.K.). M.S. is an R. D. Wright Career Development Fellow supported by the National Health and Medical Research Council, A.H.K. is an ARC Australian Postdoctoral Fellow, J.P.M. is a National Health and Medical Research Council Senior Research Fellow, and A.E.M. is an ARC Federation Fellow. We thank Alexey Kondyurin from the University of Sydney Department of Physics for assistance with and access to equipment for contact angle measurements, Chu Kong Liew for assistance with mass spectrometry, and the staff at the University of Sydney Electron Microscope Unit for help with sample preparation and microscope operation.

### References

1. Linder, M. B., Szilvay, G. R., Nakari-Setälä, T. & Penttilä, M. E. (2005). Hydrophobins: the protein-amphiphiles of filamentous fungi. *FEMS Microbiol. Rev.* **29**, 877–896.
2. Wosten, H. A., Richter, M. & Willey, J. M. (1999). Structural proteins involved in emergence of microbial aerial hyphae. *Fungal Genet. Biol.* **27**, 153–160.
3. Beever, R. E. & Dempsey, G. (1978). Function of rodlets on the hyphae of fungal spores. *Nature*, **272**, 608–610.
4. Talbot, N. J., Kershaw, M. J., Wakley, G. E., deVries, O. M. H., Wessels, J. G. H. & Hamer, J. E. (1996). MPG1 encodes a fungal hydrophobin involved in surface interactions during infection-related development of *Magnaporthe grisea*. *Plant Cell*, **8**, 985–999.
5. Temple, B. & Horgen, P. A. (2000). Biological roles for cerato-ulmin, a hydrophobin secreted by the elm pathogens, *Ophiostoma ulmi* and *O. novo-ulmi*. *Mycologia*, **92**, 1–9.
6. Wessels, J. G. H. (1994). Developmental regulation of fungal cell-wall formation. *Annu. Rev. Phytopathol.* **32**, 413–437.
7. Wösten, H. A. B., Devries, O. M. H. & Wessels, J. G. H. (1993). Interfacial self-assembly of a fungal hydrophobin into a hydrophobic rodlet layer. *Plant Cell*, **5**, 1567–1574.
8. Wosten, H. A. & de Vocht, M. L. (2000). Hydrophobins, the fungal coat unravelled. *Biochim. Biophys. Acta*, **1469**, 79–86.
9. Hakanpää, J., Linder, M., Popov, A., Schmidt, A. & Rouvinen, J. (2006). Hydrophobin HFBII in detail: ultrahigh-resolution structure at 0.75 Å. *Acta Crystallogr., Sect. D: Biol. Crystallogr.* **62**, 356–367.
10. Hakanpää, J., Paananen, A., Askolin, S., Nakari-Setälä, T., Parkkinen, T., Penttilä, M. *et al.* (2004). Atomic resolution structure of the HFBII hydrophobin, a self-assembling amphiphile. *J. Biol. Chem.* **279**, 534–539.
11. Hakanpää, J., Parkkinen, T. A. A., Hakulinen, N., Linder, M. & Rouvinen, J. (2004). Crystallization and

‡ <http://www.pdb.org>

§ <http://www.bmr.b.wisc.edu>

- preliminary X-ray characterization of *Trichoderma reesei* hydrophobin HFBI. *Acta Crystallogr., Sect. D: Biol. Crystallogr.* **60**, 163–165.
12. Hakanpaa, J., Szilvay, G. R., Kaljunen, H., Maksimainen, M., Linder, M., Rouvinen, J. *et al.* (2006). Two crystal structures of *Trichoderma reesei* hydrophobin HFBI—the structure of a protein amphiphile with and without detergent interaction. *Protein Sci.* **15**, 2129–2140.
  13. Kwan, A. H., Winefield, R. D., Sunde, M., Matthews, J. M., Haverkamp, R. G., Templeton, M. D. & Mackay, J. P. (2006). Structural basis for rodlet assembly in fungal hydrophobins. *Proc. Natl Acad. Sci. USA*, **103**, 3621–3626.
  14. Mackay, J. P., Matthews, J. M., Winefield, R. D., Mackay, L. G., Haverkamp, R. G. & Templeton, M. D. (2001). The hydrophobin EAS is largely unstructured in solution and functions by forming amyloid-like structures. *Structure*, **9**, 83–91.
  15. Fan, H., Wang, X., Zhu, J., Robillard, G. T. & Mark, A. E. (2006). Molecular dynamics simulations of the hydrophobin SC3 at a hydrophobic/hydrophilic interface. *Proteins*, **64**, 863–873.
  16. Wang, X., Permentier, H. P., Rink, R., Kruijtz, J. A., Liskamp, R. M., Wosten, H. A. *et al.* (2004). Probing the self-assembly and the accompanying structural changes of hydrophobin SC3 on a hydrophobic surface by mass spectrometry. *Biophys. J.* **87**, 1919–1928.
  17. Kwan, A. H., Gell, D. A., Verger, A., Crossley, M., Matthews, J. M. & Mackay, J. P. (2003). Engineering a protein scaffold from a PHD finger. *Structure*, **11**, 803–813.
  18. Scholtmeijer, K., Wessels, J. G. H. & Woster, H. A. B. (2001). Fungal hydrophobins in medical and technical applications. *Appl. Microbiol. Biotechnol.* **56**, 1–8.
  19. Hektor, H. J. & Scholtmeijer, K. (2005). Hydrophobins: proteins with potential. *Curr. Opin. Biotechnol.* **16**, 434–439.
  20. Schladitz, C., Vieira, E. P., Hermel, H. & Mohwald, H. (1999). Amyloid-beta-sheet formation at the air–water interface. *Biophys. J.* **77**, 3305–3310.
  21. Simmons, L. K., May, P. C., Tomaselli, K. J., Rydel, R. E., Fuson, K. S., Brigham, E. F. *et al.* (1994). Secondary structure of amyloid beta peptide correlates with neurotoxic activity *in vitro*. *Mol. Pharmacol.* **45**, 373–379.
  22. Sabate, R. & Saupé, S. J. (2007). Thioflavin T fluorescence anisotropy: an alternative technique for the study of amyloid aggregation. *Biochem. Biophys. Res. Commun.* **360**, 135–138.
  23. Butko, P., Buford, J. P., Goodwin, J. S., Stroud, P. A., McCormick, C. L. & Cannon, G. C. (2001). Spectroscopic evidence for amyloid-like interfacial self-assembly of hydrophobin SC3. *Biochem. Biophys. Res. Commun.* **280**, 212–215.
  24. Wang, X., Shi, F. X., Wosten, H. A. B., Hektor, H., Poolman, B. & Robillard, G. T. (2005). The SC3 hydrophobin self-assembles into a membrane with distinct mass transfer properties. *Biophys. J.* **88**, 3434–3443.
  25. de Vocht, M. L., Scholtmeijer, K., van der Vegte, E. W., de Vries, O. M. H., Sonveaux, N., Wosten, H. A. B. *et al.* (1998). Structural characterization of the hydrophobin SC3, as a monomer and after self-assembly at hydrophobic/hydrophilic interfaces. *Biophys. J.* **74**, 2059–2068.
  26. Wosten, H. A. B. & de Vocht, M. L. (2000). Hydrophobins, the fungal coat unraveled. *Biochim. Biophys. Acta Rev. Biomembr.* **1469**, 79–86.
  27. Vuister, G. W. & Bax, A. (1994). Measurement of four-bond HN–H alpha J-couplings in staphylococcal nuclease. *J. Biomol. NMR*, **4**, 193–200.
  28. Koradi, R., Billeter, M. & Wuthrich, K. (1996). MOLMOL: a program for display and analysis of macromolecular structures. *J. Mol. Graphics*, **14**, 51–55, 29–32.
  29. Laskowski, R. A., Rullmann, J. A., MacArthur, M. W., Kaptein, R. & Thornton, J. M. (1996). AQUA and PROCHECK-NMR: programs for checking the quality of protein structures solved by NMR. *J. Biomol. NMR*, **8**, 477–486.
  30. Van Der Spoel, D., Lindahl, E., Hess, B., Groenhof, G., Mark, A. E. & Berendsen, H. J. (2005). GROMACS: fast, flexible, and free. *J. Comput. Chem.* **26**, 1701–1718.
  31. Oostenbrink, C., Villa, A., Mark, A. E. & van Gunsteren, W. F. (2004). A biomolecular force field based on the free enthalpy of hydration and solvation: the GROMOS force-field parameter sets 53A5 and 53A6. *J. Comput. Chem.* **25**, 1656–1676.
  32. Hess, B., Bekker, H., Berendsen, H. J. C. & Fraaije, J. G. E. M. (1997). LINCS: a linear constraint solver for molecular simulations. *J. Comput. Chem.* **18**, 1431–1563.
  33. Berendsen, H. J. C., Postma, J. P. M., van Gunsteren, W. F., DiNola, A. & Haak, J. R. (1984). Molecular dynamics with coupling to an external bath. *J. Chem. Phys.* **81**, 3684–3690.